

COMPARING THE SPECTRAL REFLECTIVITY OF MINERAL RESOURCES ON
MARS FOR USE AS A PROTECTIVE EXTERIOR COATING

A THESIS SUBMITTED TO THE GEOLOGY AND GEOPHYSICS/EARTH
SCIENCES DEPARTMENT

DECEMBER 2019

By
Rachel D Bellah

Thesis Advisor
Dr Przemyslaw Dera

ABSTRACT

Thermal-reflective paints containing rutile phase titanium dioxide have been proven to reduce energy costs associated with air conditioning in sub-tropical countries like Malaysia and Brazil. In this study of spectral reflectance charts, regional composition and thermal emission spectroscopy maps of the global abundances and distribution of common Martian minerals, we identify possible in-situ analogs for a suitable replacement. There are available mineral resources that can be utilized to protect the exteriors of buildings and provide protection against heat flux for structures built on Mars. Feldspar and kaolinite were identified as possible materials for use as a protective exterior coating on Martian colonial structures. Feldspar in the sanidine or anorthite phase and kaolinite are minerals that possess higher reflectivity than rutile and titanium dioxide paint pigment, can increase the albedo of buildings, resist acidic degradation, and are both found in close proximity to Jezero and Gale Craters. Either mineral could be a sufficient exterior coating on their own, but a blend is recommended to maximize the benefits. Feldspar and kaolinite can be easily mined and incorporated into a polymer mixture during an autonomous 3D printing process.

Table of Contents

ABSTRACT	1
INTRODUCTION	4
METHODS	9
OVERVIEW OF MARTIAN SURFACE COMPOSITION	10
MARTIAN MINERAL DISTRIBUTION	12
PYROXENE	12
FELDSPAR.....	13
OLIVINE	14
SILICATES	15
ACCESSORY MINERALS.....	16
DISCUSSION	18
CONCLUSION	20
SPECTRAL REFLECTANCE CHARTS	21
WORKS CITED	22
FIGURES CITED	ERROR! BOOKMARK NOT DEFINED.

Table of Figures

FIGURE 1: REFLECTANCE SPECTRA FOR TITANIUM DIOXIDE	5
FIGURE 3: REFLECTIVITY OF COMPRESSED JSC MARS-1A , THERMAL REFLECTIVE PAINT AND CERAMIC ADDITIVE.	7
FIGURE 4: SOLAR INTENSITY INCIDENT ON THE SURFACE OF EARTH AND MARS.....	9
FIGURE 5: REGIONAL COMPOSITION MAP OF MARS.....	12
FIGURE 6: TES MAP OF GLOBAL PYROXENE ABUNDANCE.....	12
FIGURE 7: TES MAP OF GLOBAL FELDSPAR ABUNDANCE	13
FIGURE 8: TES MAP OF GLOBAL OLIVINE ABUNDANCE	14
FIGURE 9: TES MAP OF GLOBAL SILICATE ABUNDANCE	15
FIGURE 10: SPECTRAL REFLECTIVITY OF COMMON MARTIAN MINERALS.....	21

INTRODUCTION

In May 2019, NASA held the final of their 3D Printed Habitat challenge, where 30 teams created different models for possible Martian colony structures using indigenous and/or recycled materials (NASA, 2019). The goal of the challenge is to select an autonomous team to be sent to Mars to 3D print structures to prepare for human colonization. Some of the teams have submitted designs that involve machines processing the Martian regolith to use as a 3D printed concrete (Frearson, 2015). Another technique involves creating bricks that are stronger than steel-reinforced concrete by compressing the Martian regolith with the equivalent of a 10-pound hammer (Chow et al, 2017). In instances where construction requires utilization of in-situ resources, minerals with high spectral reflectivity can be extracted and processed for use as a protective, thermal-reflective coating.

Thermal reflective paint is used on roofs in sub-tropical regions like Brazil (Dornelles et al, 2011) or Southeast Asia (Al-Obaidi et al, 2014) to reduce the energy costs associated with air conditioning. Thermal reflective roof paint is considered a passive cooling technique or cool roof product, which works by preventing heat gain through radiative, reflective, convective, or conductive means (Kamal, 2012). Utilization of cool roof products can reduce the annual energy cost used by air conditioning by 28,000 mWh in industrial buildings in Singapore (Building System & Diagnostics Pte Ltd., 2011), and in the United States, consumers saved on average 30% on their energy costs (Stetiu, 1999). In addition to reducing energy loads, cool roof products can increase regional albedo which further reduces or eliminates the need to expend energy on cooling

structure interiors, leading to lower emissions and a smaller climatic impact (Dornelles et al, 2011).

Most of the currently available thermal reflective roof paint contains rutile TiO_2 , a highly infrared reflective pigment which increases opacity, durability, and the brightness of the paint (Coser et al, 2015). Rutile is the most thermodynamically stable phase of TiO_2 and also has the most compact crystalline structure, which helps to make it the most reflective phase capable of reflecting between 90-99.6% of all incoming solar radiation depending on particle size (Kumar et al, 2012). In cool pigment tests, conventional white acrylic paint containing TiO_2 outperformed other cool pigments in solar reflectance and temperature regulation (Dornelles et al, 2011). An elastomeric thermal reflective paint would be ideal for a concrete surface, as the paint is capable of stretching up to 600%, can endure 98 mph of wind-driven rain, and is mildew and dirt resistant (BEHR, 2012).

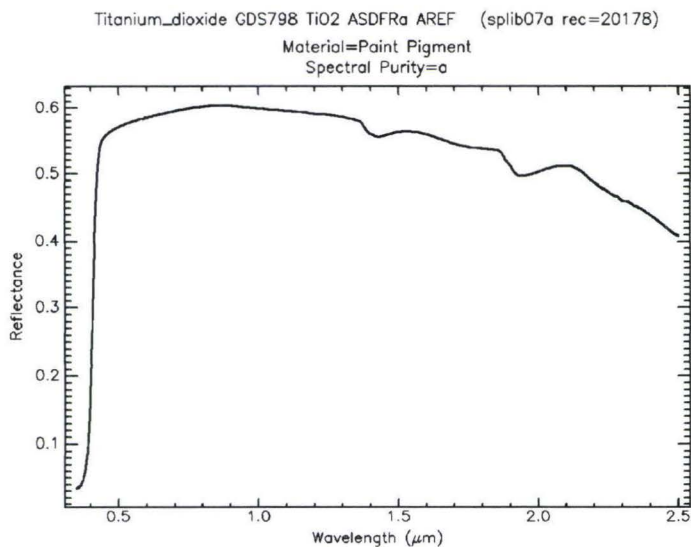


Figure 1: Reflectance spectra for titanium dioxide. From Kokaly et al, 2017.

Cool roof paints can also contain ceramic microspheres as an insulating additive. For example, Superior Products Coatings Inc. (SPCI) sells a paint that contains four

different ceramics with densities 50 times lighter than paper and claims to not only reflect all three parts of the solar spectra (ultraviolet, visible, and infrared) but to resist thermal loading (SPCI, 2013). Their ceramic blend does not absorb solar heat, reflects 92.2% of incoming visible spectrum light and 93.7% of far-infrared long waves, and contains “dead air” between the grains that blocks thermal conduction (SPCI, 2013), much like a vacuum-insulated thermos. For this study, the phases of three ceramic microsphere additives were found to be glass microspheres with a coating of mullite (Figure 2), a ceramic phase that is also used in space shuttle tiles. When added to a thermal reflective paint, the reflectivity does somewhat decrease (Figure 3). In a test of thermal insulation, glass disks and compressed chips of Martian soil simulant JSC Mars-1a coated with a paint and ceramic microsphere blend had lower bottom temperatures and a smaller difference in temperature between the top and bottom than the samples without ceramic or paint.

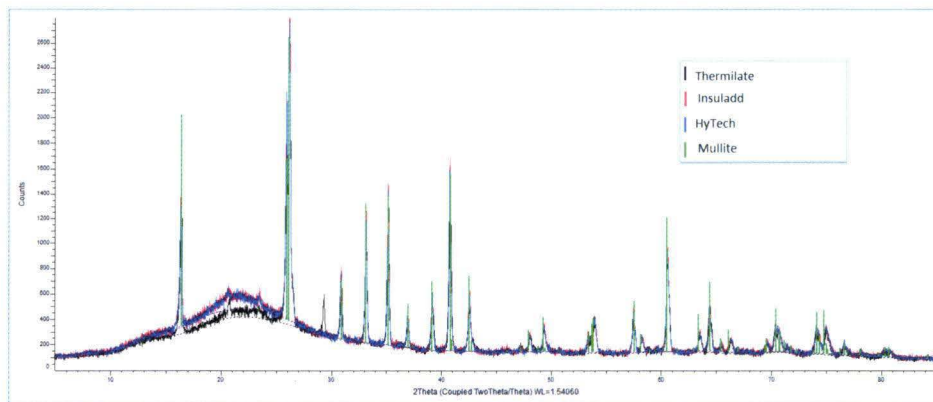


Figure 2: Top, diffraction pattern of three brands of ceramic microsphere insulating paint additive. For all three insulating sphere brands, the broad hump around 20 2θ is the signature for silica glass.

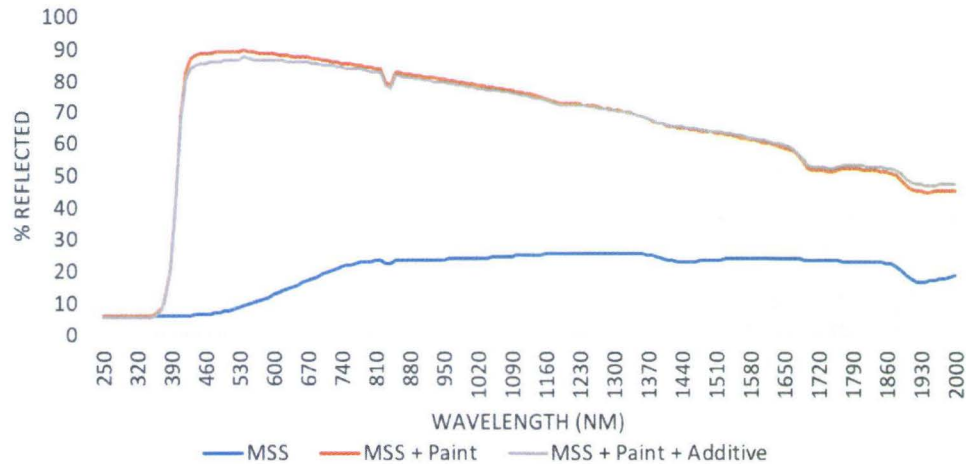


Figure 3: Reflectance of a bare compressed chip of JSC Mars-1a (blue line, MSS), JSC Mars-1a plus reflective paint (orange line, MSS + Paint), and JSC Mars-1a plus reflective paint and ceramic microsphere paint additive (gray line, MSS + Paint + Additive). Data collected in a Perkin-Elmer Lambda 1050 + UV/Vis/NIR spectrophotometer. Dip near 850 nm is due to changing detectors from dual Si to InGaS.

In keeping with NASA’s mission goals of sustainable habitation on Mars, it would be prudent to apply a protective outer layer to the colony structures to increase durability of the exterior, protect it from the elements, and reduce the need to heat or cool the interior. Titanium dioxide and ceramic microspheres have been proven to do both, but the reduction of payload weight should also be an important factor. One gallon of an elastomeric thermal reflective paint can weigh around 12 pounds and containers of ceramic additive are sold by the pound, with one pound of ceramic additive going into one gallon of paint. A good gallon of paint can cover 125 square feet, which is about one average sized room.

If a product similar to thermal reflective paint or ceramic microspheres is to be used as a protective coating for Martian structures, it would amount towards a significant portion of the payload and would need to be replenished with supply drops as the Martian population grows and expands. SpaceX’s Falcon Heavy can carry 37,000 lbs of payload to Mars, and their Starship (maiden orbital flight projected for 2020) is being designed to

eventually replace the Falcon Heavy and carry over 100 tons of payload (SpaceX, 2019). Even with the large capacities of the rockets, there is no need to waste payload space when a similar product can be made with minerals found on the surface of Mars.

NASA's geologic criteria for landing site selection took into account several different factors: the landing site must have evidence of subaqueous or hydrothermal sediments or hydrothermally altered rocks, it must have minerals in the aqueous phase like phyllosilicates in an outcrop, access to raw and unaltered rock, and either be Noachian or early Hesperian in age (Grant and Golombek, 2018). NASA announced their landing site selection as Jezero Crater (Grant and Golombek, 2018), just southeast of Nili Fossae. Jezero Crater includes a river delta and possibly formerly lacustrine sediments, Mg-enriched carbonate rocks and phyllosilicate-bearing deposits (Grant and Golombek, 2018). The presence of both carbonates and phyllosilicates goes against the TES map abundances but proves that there needs to be more in-depth global geologic and mineralogic surveys of the Martian surface rather than just a birds-eye-view.

Another consideration for designing energy-efficient solutions for future Mars colonies is the amount of sunlight incident on the surface of Mars. The air is saturated with dust, which helps to reduce the intensity of the sun at the surface. Because Mars is further away from the sun than Earth, it receives less than half of the sunlight compared to Earth does. As seen in Figure 4, the intensity of the sun that reaches the surface of Mars at a 30-degree zenith is only ~33% of AM0, and at a 60-degree zenith the intensity is reduced to ~17% (Edmonson et al, 2005). AM0 is the measure of light that has not interacted with an atmosphere. The average temperature on Mars is -63°C (Williams, 2018), with noontime equatorial temperatures reaching ~20°C and the warmest soil

temperature recorded as 27°C from the Viking Orbital Infrared Thermal Mapper (Tillman, 2001). There is less pressure to prevent heat gain, but protective coatings are still necessary to mitigate UV damage to outdoor walls on Martian colony buildings.

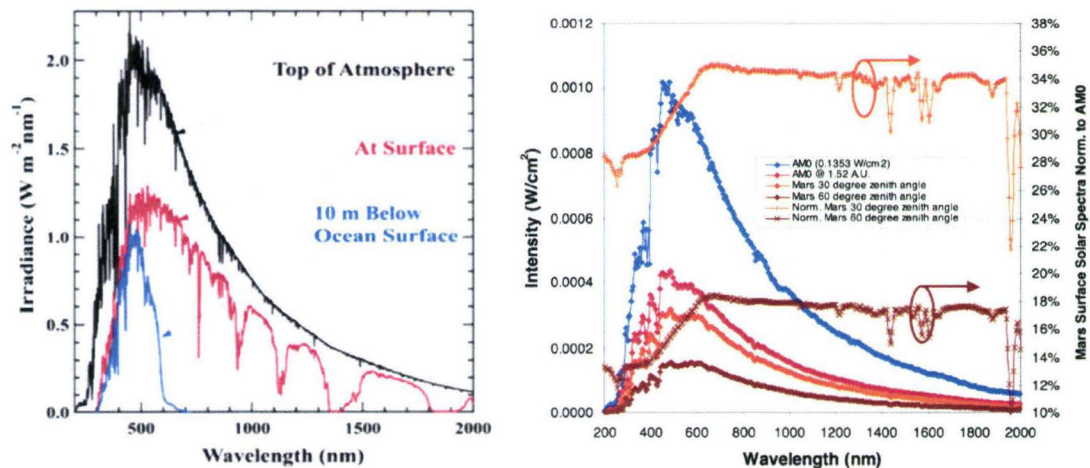


Figure 4: Left, a graph displaying the intensity of the sun incident on the atmosphere, surface, and 10m below the ocean surface on Earth. From Shapley, 2012. Right, a graph displaying the intensity of the sun incident on the surface of Mars taken from 30° and 60° solar angle zeniths using Crisp and MER data. From Edmonson, et al, 2005.

METHODS

Reference spectral reflectance data for Martian minerals were taken from the USGS Spectral Library, Version 7. The library includes special codes associated with sample quality and the type of instrument the sample was tested in. BECK stands for a Beckmann 5270 spectrometer, which measures reflectivity in the 0.2 - 3 μm range; ASDFR stands for ASD Full Range spectrometers covering 0.35 – 2.50 μm (Kokaly et al, 2017). The letter codes for spectral purity are as follows: “a” means the sample is pure with no contaminants present; “b” means that the spectrum appears pure but other tests have found contaminants that don’t affect the reflectivity; “c” means that the spectrum has features that come from contaminants (Kokaly et al, 2017). Attention was paid to the grade of the mineral as well as the phase name stated on the charts; spectra for this paper

were selected based on the highest grade available. Broad-range spectra (from 1.12 – 216 μm) were avoided since they extended well outside of the infrared range of 0.70 – 1.10 μm and the full range of 0.70 – 2.50 μm .

Diffraction data for three ceramic microsphere insulating paint additive brands, seen in Figure 2, was collected using a Bruker D8 Advance powder diffractometer. Spectral reflectance for TiO₂-containing thermal reflective paint (BEHR Elastomeric Masonry and Stucco Paint), with and without an insulating ceramic microsphere paint additive (Insuladd), was obtained using a Perkin-Elmer Lambda 1050 + UV/Vis/NIR spectrophotometer. Chips of JSC Mars-1a were compressed in a manual pump hydraulic press under ambient conditions at 50 MPa.

OVERVIEW OF MARTIAN SURFACE COMPOSITION

Thermal emission spectroscopy (TES) data has been used to map the composition and mineralogy of the upper 10 microns of low-dust portions of the Martian surface. Spectroscopy has found that the surface of Mars is not homogeneous, and there are significant variations in the abundances of minerals from one distinct region to another, suggesting that the mineralogical variations depend on bedrock mineralogy rather than alteration (Rogers and Christensen, 2007). The older southern highlands are dominated by basalt, whereas the younger northern plains are primarily andesitic to basaltic andesite, or a basalt with a high silica or poorly crystalline phase (Rogers and Hamilton, 2015; Rogers and Christensen, 2007; Christensen et al, 2001). Primary Martian minerals are pyroxene, olivine, plagioclase or alkali feldspar, and silicates (Mangold et al, 2019; Rogers and Christensen, 2007; Bandfield, 2002). Carbonates and quartz or amphibole are

not found above the 0.1 detection limit anywhere on the maps, and only a few pixels in Acidalia have sulfate abundances above the detection limit (Bandfield, 2002).

TES maps are not the only tool to use when deciphering the composition of the Martian surface. Regions can also be coded depending on overall composition, as done by Rogers and Hamilton, 2014, based on the data from Rogers and Christensen (2007), seen in Figure 5. Using regional composition maps can help settlers and autonomous builders to locate minerals necessary for the construction process. Each pixel on the map is color coded based on the dominant composition. RC Group 1 consists of 33 % high-silica phases, 30% plagioclase, 15% LCP, 6% HCP, 4% olivine, and 12% “other”, and is most prevalent in Northern Acidalia and Solis Planum; RC Group 2 consists of 31% plagioclase, 29% HCP, 12% high-silica phases, 7% olivine, 4% LCP, and 17% “other”, and is most prevalent in Syrtis Major; RC Group 3 consists of 25% plagioclase, 20% HCP, 18% high-silica phases, 11% olivine, 10% LCP, and 16% “other”, and is most prevalent in Tyrrhena Terra, Cimmeria Terra, Hesperia Planum, and Sinus Meridiani; and RC Group 4 consists of 36% plagioclase, 20% HCP, 19% high-silica phases, 6% LCP, 4% olivine, and 15% “other, and is most prevalent in Aonium-Phruxi and Mare Sirenum (Rogers and Christensen, 2007). The compositional groups are not limited to the regions they are most prevalent in. The compositional groups do not go into high detail beyond identification of dominant mineral phase, but they can be used as a starting point.

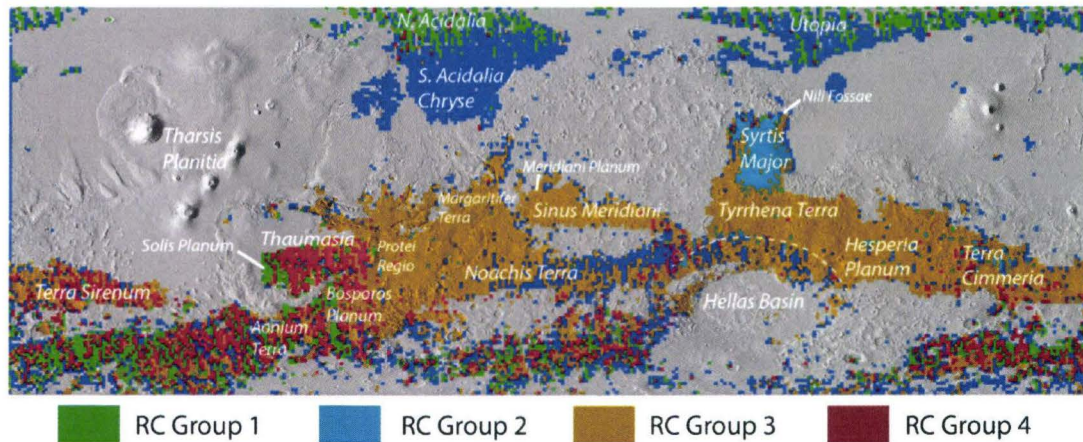


Figure 5: Regional composition map of Mars, with notable regions labeled. From Rogers and Hamilton, 2014.

MARTIAN MINERAL DISTRIBUTION

Pyroxene

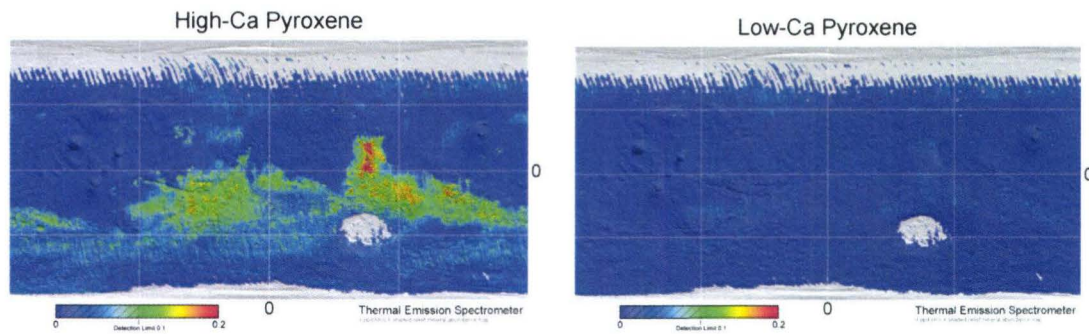


Figure 6: TES maps of Mars displaying high-Ca pyroxene abundance (left) and low-Ca pyroxene abundance (right). From Bandfield, 2002.

Pyroxene is subdivided into high-Ca pyroxene, referred to as either HCP or clinopyroxene, and low-Ca pyroxene, referred to as LCP or orthopyroxene (Bandfield, 2002). HCP is the dominant phase, with the highest concentration in Syrtis Major. In high latitude, low-albedo regions, the maximum abundance is ~ 0.1 , whereas the concentration in equatorial low-albedo regions can reach up to 0.2 (Bandfield, 2002). HCP concentrations are uniformly high in Syrtis Major, Tyrrhena Terra, western Cimmeria Terra, and in portions of Margaritifer Terra and Thaumasia Planum (Rogers and

Hamilton, 2015). HCP concentrations are uniformly low in the lowlands, southern high latitude, and the northern rim of Hellas basin (Rogers and Hamilton, 2015). The phases of HCP that have been identified by CheMin are pigeonite $((\text{Mg}, \text{Fe}, \text{Ca})_2\text{Si}_2\text{O}_6)$ with Ca atomic 5-25%, and augite $((\text{Ca}, \text{Mg}, \text{Fe})_2\text{Si}_2\text{O}_6)$ with Ca atomic \sim 50% (Morrison et al, 2018).

LCP has primarily low concentrations planetwide and is below the 0.1 detection limit, except for in low-albedo regions of the northern hemisphere where the concentrations can be between \sim 0.05-0.1 (Bandfield, 2002). LCP concentrations are uniformly low in Syrtis Major and Thaumasia Planum, and relatively low in Tyrrhena Terra, Hesperia Planum, and Sinus Meridiani (Rogers and Hamilton, 2015). The orthopyroxene phase that has been identified by CheMin in Gale Crater is $(\text{Mg}, \text{Fe}, \text{Ca})_2\text{Si}_2\text{O}_6$ (Morrison et al, 2018). LCP-enriched outcrops are only found in Noachian age terrain (Rogers and Christensen, 2007).

Feldspar

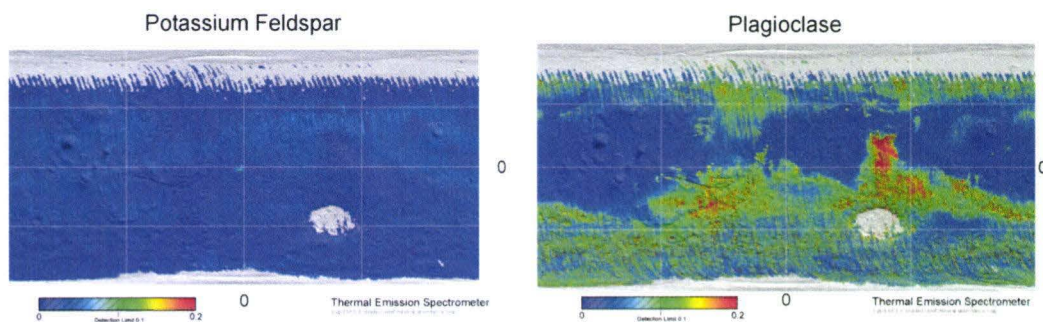


Figure 7: TES map showing abundances of alkali feldspar (left) and plagioclase feldspar (right). From Bandfield, 2002.

Feldspar minerals can be separated into two categories: alkali feldspar and plagioclase feldspar. Alkali feldspars are not present in significant abundance across the map and are not found in concentrations above 0.07 (Rogers and Christensen, 2007;

Bandfield, 2002). The lowest concentration of feldspar can be found in Sinus Meridiani (Rogers and Hamilton, 2015). In the northern hemisphere, alkali feldspars are usually found in concentrations ~ 0.05 (Bandfield, 2002). Lava flows in northern and eastern Syrtis Major are enriched in feldspar relative to flows in the southern and central areas (Rogers and Hamilton, 2015). South Acidalia Planitia and Cerberus Fossae have lower than average feldspar concentration, and northern Acidalia Planitia has higher than average feldspar concentration (Rogers and Hamilton, 2015). In Gale Crater, alkali feldspar has been identified by CheMin in the sanidine phase ($K_{0.74}Na_{0.26}Al_1Si_3O_8$) (Morrison et al, 2019). Plagioclase feldspar is found in significant concentrations over all low-albedo regions and has been identified as intermediate to calcic in composition (Morrison et al, 2019; Banfield, 2002). The average concentration of plagioclase found in Gale Crater that has been identified by CheMin is anorthite An_{40} ($Ca_{0.4}Na_{0.6}Al_{1.4}Si_{2.6}O_8$) (Morrison et al, 2019), with concentrations ~ 0.05 - 0.15 in high-latitude low-albedo regions, and ~ 0.1 - 0.2 in equatorial low-albedo regions (Bandfield, 2002).

Olivine

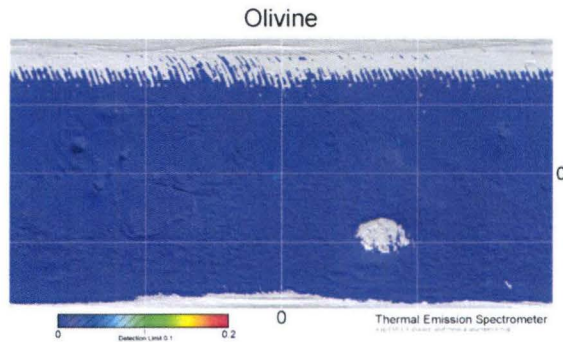


Figure 8: TES map of global olivine abundance. From Bandfield, 2002.

Olivine is not present in significant quantities, as older studies (Banfield, 2002) found global olivine to be under the detection limit. Rogers and Hamilton (2015) added mid-range olivine compositions to the database, rather than just looking for the forsterite/fayalite end members, and still found lower abundances than expected for a primarily igneous planet. Possible explanations for this lack could lie in aqueous alteration, as olivine is very quick to dissociate in the presence of water (Morrison et al, 2019). Global olivine abundance is under ~ 0.05 (Banfield, 2002), with exceptions to the rule being globally elevated olivine abundances co-occurring with globally elevated HCP in Nili Fossae, Cimmeria Terra, Margaritifer Terra, in some southern high latitude crater deposits, and inter-crater plains located in Tyrrhena Terra (Rogers and Hamilton, 2015). The average olivine composition at Gale Crater is $\text{Mg}_{1.21}\text{Fe}_{0.76}\text{Mn}_{0.02}\text{Ca}_{0.01}\text{SiO}_4$, similar to the average olivine composition of Martian meteorites (Morrison et al, 2019), and the olivine phase with the highest global maximum abundance is Fo_{68} (Rogers and Hamilton, 2015).

Silicates

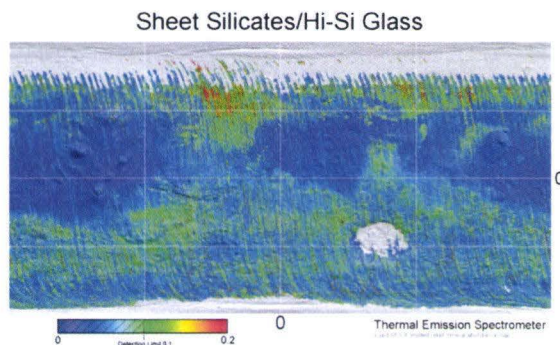


Figure 9: TES map showing the abundance and range of silicates on Mars. From Banfield, 2002.

High-silica phases consist of the combined abundances of phyllosilicates, obsidian or interstitial glass, zeolites, poorly crystalline weathered rind materials, and opals (Rogers and Christensen, 2007). Sands in Gale Crater are 24% plagioclase, 22% pyroxene, 35% glass and amorphous phase, and a large part of northern plains might be glass rich sand instead of high plagioclase andesite (Mangold et al, 2019). Central peaks in large impact craters can have hydrated silicates, which are enriched in sulfur and chlorine in dunes, suggesting aerosol contamination (Mangold et al, 2019). Globally, sheet silicates and high-silica glass are fairly abundant, even in high-dust areas (dark blue on TES maps). High-silica phase abundance is highest in northern hemisphere regions such as Acidalia Planitia, Utopia Planitia, portions of Thaumasia, Aonium Planum, and Bosporous Planum, and the lowest in western Noachis Terra, Tyrrhena Terra, portions of Cimmeria Terra, and northern Syrtis Major (Rogers and Hamilton, 2015).

Accessory Minerals

Other minerals found in significantly smaller regions, either due to reality or equipment limitations, or in significantly lower abundances than the minerals discussed above will be lumped into this section. However, it is important to keep in mind that TES only detects the upper 10 microns of the crust and is not a reflection of subsurface mineral abundances, and mineral abundances may be different even a few centimeters below the surface. The minerals briefly described below are not expected to be in a physical abundance high enough to be utilized on a massive scale as a possible reflective outer coating but may be utilized either as a constituent in a mineral mixture or as an ingredient for a regolith-based building material.

Hematite is only identified above the TES detection limit in two places: Sinus Meridiani, where it is detected between 0.1 – 0.2, and a singular pixel within Aram Chaos where it is detected between 0.1 – 0.15 (Bandfield, 2002). Iron oxides roughly 10 cm thick, mostly consisting of hematite, have been found on the surface of Mars Hematite blueberries have also been found by Opportunity (Mangold et al, 2019).

Clays and other aluminosilicates are mostly produced by weathering processes on the surface (Mangold et al, 2019). They can be found in weathered regions like Mawrth Vallis, where Al-rich kaolinite is detected on top of Fe/Mg-rich smectite clays, mostly in the nontronite phase (Mangold et al, 2019). Clays have also been detected primarily in Noachian crust, sedimentary rocks, and presumably lacustrine sediments, and while clay has been found in Hesperian and Amazonian crust it is limited to regional activity (Mangold et al, 2019).

Sulfates can be found in bedrock, equatorial layered deposits, in eolian deposits around the northern polar cap, and in association with iron hydroxides (Mangold et al, 2019). The presence of sulfates implies that a sulfur source is required, either from volcanic outgassing or sulfide alteration in the form of pyrite (Mangold et al, 2019). Sulfates have been found in concentrations of ~0.05 – 0.1 in equatorial low-albedo regions, a handful of pixels in Acidalia, and scattered through the north polar sand seas (Bandfield, 2002). Local deposits of a sulfate phase jarosite, a K/Na-Fe sulfate that only forms when $\text{pH} < 4$, have been found in Meridiani Planum (Mangold et al, 2019).

Carbonates have not been found with TES above the detection limit anywhere on the map, and most areas that show any carbonate signature at all are dominated by 0 – 0.05 abundance (Bandfield, 2002). Carbonates should be found in higher abundance to

compensate for the loss of atmosphere, but unfortunately that is not the case as carbonates are somewhat limited to where they are dug up or exposed in an outcrop (Mangold et al, 2019). In Nili Fossae and Jezero Crater, hydromagnesite, a Mg-rich carbonate related to alteration of olivine-rich bedrock, was detected by CRISM (Mangold et al, 2019; Grant and Golombek, 2018).

Quartz and amphibole are not found above the detection limit in any of the study areas, and most surfaces only register about 0 – 0.01 for both minerals (Bandfield, 2002), and likely only exists in small local outcrops undetectable by TES (Rogers and Christensen, 2007). However, quartz may be found in subsurface pockets similar to Earth.

DISCUSSION

The goal of identifying a prospective local source of a reflective exterior additive for Martian buildings is to find a mineral with spectral reflectance that closely matches the curve of titanium dioxide paint pigment, seen in Figure 1 and Figure 10-H. It covers nearly the full spectrum of light, and more importantly reflects almost 60% of incoming light. When used in paint on a substrate, the reflectivity increases to over 90%, seen in Figure 3. A prospective reflective additive mineral must have an “uneventful” reflectance spectrograph, with no large dips that could degrade the performance of the protective outer coating. Ideally, the minerals that can be used as a protective reflective outer coating will be in relative high abundance and within autonomous rover distance from the landing site.

Jezero Crater and Nili Fossae have been found to carry Mg-enriched carbonates (hydromagnesite, which is not found in the USGS Spectral Library) and phyllosilicates.

Kaolinite (Figure 10-F) has very high reflectivity, is naturally white in color and opaque, small particle size, and is generally easy to work with as most clay minerals are. One downside is that kaolinite's reflective spectrum is not as uniform as sanidine, anorthite, or titanium dioxide paint pigment, and it decreases sharply at 1.5 μm and more gradually after 2.0 μm . While this is not dissimilar to titanium dioxide paint pigment, it is much more drastic.

Feldspars are commonly used in industrial applications to make drinking glasses and floor tiles, as a fluxing agent to reduce melting temperature when creating glass or ceramics, and can be used as a filler in paint to increase weathering resistance (IMA Europe, 2011). The angular nodular shape and tight packing provides high abrasion resistance (¹PCI, 2003). Feldspars can also be used in conjunction with resin to create highly transparent films that are very resistant to abrasion and scratching, and thermal management LDPE films that reflect heat in agricultural applications (Zilles, 2016). While not nearly as neat as rutile TiO_2 , needle-shaped feldspar crystals have been found in nakhilites (McSween and Huss, 2010), and milled feldspar is composed of nodular angular particles which can interlock and pack tightly when used as a filler (¹PCI, 2003).

Kaolinite has been used industrially as an inert filler and a pigment extender or replacement for TiO_2 pigment due to its whiteness, opacity, and hydrophilic properties (²IMA Europe, 2011; ²PCI, 2003). Calcined kaolin can be used in paints to increase the opacity, albedo, and flake resistance (²IMA Europe, 2011). In polymerized material, kaolin can be added to reduce shrinkage and cracking during formation, and kaolin can be added to thin films to improve infrared absorption (²IMA Europe, 2011). Mullite can

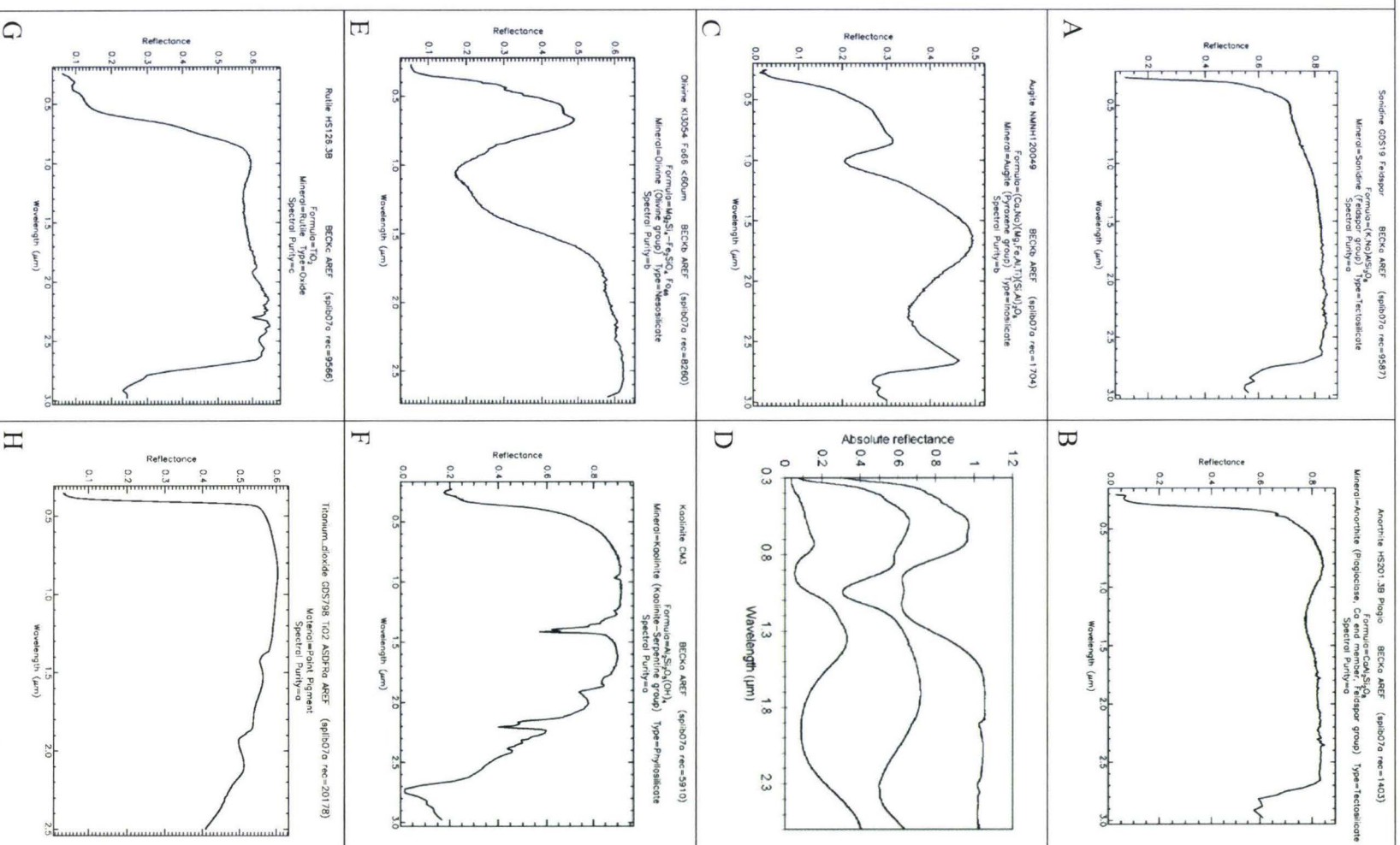
be derived from kaolin by calcining it past 1200°C (IMA Europe, 2011). Kaolinite's platy structure

CONCLUSION

Based purely on spectral reflectance and global abundance alone, feldspars in the sanidine (Figure 10-A) and anorthite (Figure 10-B) phases would make ideal candidates for a reflective shell. Anorthite is globally more abundant than sanidine, but sanidine has a steadier reflectivity across the entire light spectrum and the reflectance pattern is very similar to titanium dioxide paint pigment. Anorthite experiences a slight dip between 1.0 – 1.5 μm , but overall the reflectance hovers around 80%. Sanidine has been positively identified in Gale Crater, but unfortunately Gale is quite a distance from Jezero Crater, which might take it out of the running depending on how far autonomous builders are willing or able to go in order to harvest raw material. Anorthite, or plagioclase feldspar in general, is abundant near Jezero Crater and Nili Fossae. Kaolinite has been observed on the surface by Curiosity in Gale Crater, making access to clay pockets extremely easy. Because of the proximity to the landing site of Mars 2020, the ease of use, and physical properties, kaolinite might be much more suited to be used as a protective and reflective outer coating on Martian settlements than any other mineral examined in this study. Kaolinite can be harvested and utilized as an additive in building polymers, and calcined to turn into mullite, which is an effective insulator at extreme temperatures. A blend of kaolinite and feldspar has the potential to be a low-cost, in-situ alternative to bringing reflective and insulating coatings to Mars.

SPECTRAL REFLECTANCE

Figure 10: Reflectance spectra from common Martian mineral phases. A- feldspar in the sanidine phase. B- feldspar in the anorthite phase. C- pyroxene in the augite phase. D- three pyroxenes: The top line is vertically offset by +0.2 and is HCP $FS_{10}EN_{40}WO_{50}$; the middle line is a Type B HCP $FS_{2}EN_{49}WO_{49}$; the bottom is an LCP $FS_{41}EN_{55}WO_{4}$. E- olivine FO_{66} , which was the closest relative to FO_{68} which is found on Mars. F- kaolinite clay. G- rutile TiO_2 . H- TiO_2 paint pigment. D is from Cloutis, 2002; all other spectra are from Kokaly et al, 2017.



Works Cited

Al-Obaidi, K. M., Ismail, M., Abdul Rahman, and A. M., 2014, Passive cooling techniques through reflective and radiative roofs in tropical houses in Southeast Asia: A literature review: *Frontiers of Architectural Research*, v. 3, pp 283-297, <http://dx.doi.org/10.1016/j.foar.2014.06.002>

Bandfield, J. L., 2002, Global mineral distributions on Mars: *Journal of Geophysical Research*, v. 107, no. E6, <https://doi.org/10.1029/2001JE001510>

Bedinger, G. M., 2019, Titanium and Titanium Dioxide, in *Mineral commodity summaries 2019*, U. S. Geological Survey, pp 174-175, <https://doi.org/10.3133/70202434>

BEHR, 2012, *Elastomeric Masonry, Stucco & Brick Paint*, <https://www.behr.com/consumer/products/specialty-paint/masonry-stucco-and-brick-paint/behr-premium-elastomeric-masonry-stucco-and-brick-paint>

Building System & Diagnostics Pte Ltd., 2011, *COOL Roofs in Apec Economies: Review of Experience, Best Practices and Potential Benefits*: <http://esci-ksp.org/wp/wp-content/uploads/2012/03/Cool-Roofs-in-APEC-Economies.pdf>

Chow, B. J., Chen, T., Zhong, Y., and Qiao, Y., 2017, Direct Formation of Structural Components Using a Martian Soil Simulant: *Scientific Reports*, v. 7, <http://dx.doi.org/10.1038/s41598-017-01157-w>

Christensen, P. R. et al, 2001, Mars Global Surveyor Thermal Emission Spectrometer experiment: Investigation description and surface science results: *Journal of Geophysical Research*, v. 106, no. E10, pp. 23, 823-23, 871, <https://doi.org/10.1029/2000JE001370>

Coser, E., Moritz, V. F., Krenzinger, A., and Ferreira, C. A., 2015, Development of paints with infrared radiation reflective properties: *Polimeros*, v. 25, i. 3, pp 305-310, <http://dx.doi.org/10.1590/0104-1428.1869>

Dornelles, K. A., Roriz, M., Roriz, V. F., and Caram, R. M., 2011, Thermal Performance of White Solar-Reflective Paints for Cool Roofs and the Influence on the Thermal Comfort and Building Energy Use in Hot Climates: Proceedings of the ISES Solar World Congress 2011, <http://dx.doi.org/10.18086/swc.2011.02.02>

Edmonson, K. M., Joslin, D. E., Fetzer, C. M., King, R. R., Karam, N. H., Mardesich, N., Stella, P. M., Rapp, D., Mueller, R., 2005, Simulation of the Mars surface solar spectra for optimized performance of triple junction solar cells: 19th SPRAT Conference, Cleveland, OH, <https://trs.jpl.nasa.gov/bitstream/handle/2014/37746/05-2732.pdf?sequence=1>

Frearson, A., 2015, Foster + Partners reveals concept for 3D-printed Mars habitat built by robots: *dezeen*, <https://www.dezeen.com/2015/09/25/foster-partners-concept-3d-printed-mars-habitat-robots-regolith/>

Grant, J., and Golombek, M., 2018, Final Letter describing the outcome of the 4th Mars 2020 Rover Landing Site Workshop: Smithsonian National Air and Space Museum, https://marsnext.jpl.nasa.gov/workshops/2018-10/M2020_LSW_FinalOutcomeLetter_for_MMeyer_181023.pdf

¹IMA Europe, 2011, Feldspar Fact Sheet: Industrial Minerals Association – Europe, https://www.ima-europe.eu/sites/ima-europe.eu/files/minerals/Feldspar_An-WEB-2011.pdf

²IMA Europe, 2011, Kaolin Fact Sheet: Industrial Minerals Association – Europe, https://www.ima-europe.eu/sites/ima-europe.eu/files/minerals/Kaolin_An-WEB-2011.pdf

Kamal, M. A., 2012, An overview of passive cooling techniques in buildings: Design concepts and architectural interventions: Acta Technica Napocensis: Civil Engineering & Architecture, v. 55, n. 1

Kokaly, R. F., et al, 2017, USGS Spectral Library Version 8: U. S. Geological Survey Data Series 1035, 61p, <https://doi.org/10.3133/ds1035>

Kumar, S., Verma, N. K., and Singla, M. L., 2012, Size Dependent Reflective Properties of TiO₂ Nanoparticles and Reflectors Made Thereof: Digest Journal of Nanomaterials and Biostructures, v. 7 i. 2, pp 607-619

Mangold, N., Flahaut, J., and Ansan, V., 2019, The Surface Composition of Terrestrial Planets: Oxford Research Encyclopedia, Planetary Science, 62 p, <http://doi.org/10.1093/acrefore/9780190647926.013.105>

McSween, H. Y. Jr., Huss, G. R., 2010, Meteorites: a record of nebular and planetary processes *in* Cosmochemistry, Cambridge University Press, pp 157 - 191

Morrison, S. M. et al, 2018, Crystal chemistry of martian minerals from Bradbury Landing through Naukluft Plateau, Gale crater, Mars: American Mineralogist, v. 103, pp 857-871, <https://doi.org/10.2138/am-2018-6124>

NASA, 2019, 3D Printed Habitat Design Challenge, https://www.nasa.gov/directorates/spacetech/centennial_challenges/3DPHab/index.html

¹PCI, 2003, Feldspar and Nepheline Syenite Fillers with a Purpose: Paint & Coatings Industry, <https://www.pcimag.com/articles/83031-feldspar-and-nepheline-syenite-fillers-with-a-purpose>

²PCI, 2003, Kaolin Clay: Functional Optical Additives: Paint & Coatings Industry, <https://www.pcimag.com/articles/83344-kaolin-clay-functional-optical-additives>

Rogers, D. A., and Christensen, P. R., 2007, Surface mineralogy of Martian low-albedo regions from MGS-TES data: Implications for upper crustal evolution and surface alteration: *Journal of Geophysical Research*, v. 112, E01003, <https://doi.org/10.1029/2006JE002727>

Rogers, D. A., and Hamilton, V. E., 2015, Compositional provinces of Mars from statistical analyses of TES, GRS, OMEGA and CRISM data: *Journal of Geophysical Research: Planets*, v. 120, pp 62-91, <http://doi.org/10.1002/2014JE004690>

Shapley, P., 2012, *The Ozone Layer*: University of Illinois, <http://butane.chem.uiuc.edu/pshapley/GenChem2/A2/1.html>

SPCI, 2013, *Sunshield Product Information*: Superior Products Coatings Inc., <https://www.spcinfo.com/documents/sunshield.pdf>

SpaceX, 2019, *Making Life Multiplanetary*: SpaceX, <https://www.spacex.com/mars>

Stetiu, C., 1999, Energy and peak power savings potential of radiant cooling systems in US commercial buildings: *Energy and Buildings*, v. 30, i. 2, pp 127-138, [https://doi.org/10.1016/S0378-7788\(98\)00080-2](https://doi.org/10.1016/S0378-7788(98)00080-2)

Tillman, J. E., 2001, *Mars Temperature Overview*: University of Washington, http://www-k12.atmos.washington.edu/k12/resources/mars_data-information/temperature_overview.html

Williams, D. R., 2018, Mars Fact Sheet: NASA,
<https://nssdc.gsfc.nasa.gov/planetary/factsheet/marsfact.html>

Zilles, J. U., 2016, Feldspar and Syenites *in* Polymers and Polymeric Composites:
A Reference Series, pp 1-14, https://doi.org/10.1007/978-3-642-37179-0_5-6